

The Effects of Vein Morphology on Elastic Wing Deformation

Yosef Mendelson

Under the close supervision of Dr. Gal Ribak

School of Zoology, Tel Aviv University

Submission date: September 2022

Abstract:

Unlike flying vertebrates, insect flight relies on the passive, elastic deformation of their wings to generate lift. To do so, wing aerofoil shape is distorted by the aerodynamic and inertial forces acting on their unique and intricate mechanical properties. The complex interplay between these factors complicate previously proposed mathematical models that try to understand the benefits native to more rigid or more elastic wings. In our study we focus on elastic deformation and lift generation as a function of vein morphology and wing flexural rigidity. By synthetically replicating the wings of the *Protaetia cuprea* and solely fortifying their veinal network, we are able to directly assess the implications of flexural stiffness on wing deformation and its aerodynamic influences. Our results conclude that a change to vein cross-sectional area directly effects wing rigidity and thus, deformation capabilities. Furthermore, our results provide insight pertaining to important factors to take into consideration when synthetically remodeling authentic flapping wings.

Deleted: *Cuprea*

Formatted: Font: Italic, Complex Script Font: Italic

1. Introduction:

For millions of years, wings have been subject to evolution through natural and sexual selection. Their divergence and gradual morphological advances directly impact both maneuverability and the energetic efficiency of flight in different species¹. Unlike flying vertebrates, insects lack musculature in their wings which otherwise offer active and precise, aerodynamically favorable alterations during flight². Instead, during flapping, insects rely on the more passive elastic deformation of their thin, membranous wings. In this case, the aerofoil shape of the malleable insect wings is controlled by their interactions with inertial and aerodynamic forces as they flap³.

Passive deformation in insects is further regulated by mechanical properties throughout the wings such as a relatively rigid veinal network, used to provide deformation-supporting and deformation-limiting areas². Different venation patterns thus translate into

differences in wing twist and camber, pushing species to adopt different niches depending on what their wings are better suited for. One such example was seen when comparing between interspecific wing-vein arrangements and the resulting elastic deformation within the scarab beetle family. Rose chafers, which require precision-landing to feed on flowers, were found to have a subtle difference in vein arrangement leading to a more compliant trailing edge (TE). In contrast, dung beetles, who use fast flight to reach a general feeding ground area, expressed a shift in wing-vein placement resulting in a more locally rigid wing with less deformation^{1,4}. It is at this intersection that controversy still remains whether these elastic deformations improve or stunt aerodynamic output in comparison to a more rigid alternative.

In an attempt to understand the functional significance of wing venation on flexural rigidity (EI), Combes and Daniels (2003) took a quantitative approach using a simple cantilever beam model to measure the flexural rigidity of insect wings. They concluded that flexural rigidity, and consequently, span-wise and chord-wise deflection scales with the size of the individual⁵. Studies by Meresman and Ribak (2017), however, debated that morphological parameters do not change evenly with changes to body size. This renders simplistic mathematical models unfavorable when trying to inspect the tradeoffs between having a more rigid or compliant wing³.

Here, we aimed to circumvent the lack of isometric growth, and complexity of the material properties, typical of free-flying beetles in order to directly determine the effects of flexural rigidity on wing deformation and lift generation. By replicating the wings of *Protaetia cuprea* (Rose Chafer beetle) and modifying their veinal cross-sectional areas, we were able to manipulate wing rigidity while nullifying the effects other factors (materials, size, wing vein arrangement) contributing to mechanical properties. Our study thus steers away from generic and oversimplified mathematical predictions in the hopes of understanding the complexities behind compliant versus rigid wings and their aerodynamic influence.

Deleted: YEAR

Formatted: Highlight

Formatted: Highlight

Deleted: Yonatan

Deleted: Gal

Deleted: YE

Deleted: AR

Deleted: in

Deleted: models

Formatted: Font: Italic, Complex Script Font: Italic

Deleted: C

Deleted: only

Deleted: directly

Deleted: all

2. Materials and Methods:

2.1 Wings

3 sets of 3D-printed, scaled-up replicas (1:⁵) of Rose Chafer wings, fitted with mounting-stalks specific to the flapper device, (see section 2.2) were obtained from Or Filc who is manufacturing these wings as part of her MSc. Research in the lab (in collaboration with the school of Mechanical Engineering). Each wing-set represented a different shape of veinal cross-sectional area, herein; horizontal, round, and vertical (labeled H, O and V respectively) geometry. The rest of the wings' morphological and mechanical properties remained identical. Six natural morphological landmarks comprising wing edge-vein junctions and intervein joints: the wing tip (wt), marginal-joint (mj), radius-posterior (RP), media-posterior (MP), cubitus-anterior (CuA) and analis-anterior (AA) were marked with white dots on each wing using acrylic paint (see figure 1a and c.) to allow their accurate tracking using high-speed films (obstruction to flapping kinematics due to paint was considered negligible in this experiment). The seventh point, referred to as the wing-base (wb), was considered to be the gear of the flapper directly above the wing clasp.

Deleted: 6

Deleted: in collaboration with the School of Engineering

Deleted: .

2.2 Flapper and Load Cell

The Flapper (figure 1d.), a custom-made contraption whose motor is powered by a battery, was provided by Leeor Mordoch who is developing the flapping mechanism as part of his MSc research in the lab (in collaboration with the School of Mechanical Engineering). The flapper was secured onto a Zemic L6B-L load cell measuring the total weight of the flapper + wings.

Deleted: and

Deleted: the

Clasps on both sides were custom fitted to secure the synthetic wings such that the wings were sustained by screws to ensure no variation in the wing offset or wing pitch. The flapper was made to flutter the synthetic wings back and forth at 4 speeds powered by 0.3V, 0.5V, 0.7V and 0.9V while the Zemic L6B-L load cell simultaneously recorded the lift force generated by the flapping. A screwdriver was used to gently press down on the load cell at the start of each recording to indicate the starting point. Frame numbers of the videos were then synchronized

with the time stamp of the force measurement of the load cell (which measured weight every 10 milliseconds) and the lift force measurements between the starting frame to the end frame were averaged.

Deleted: converted to
Deleted: s
Deleted: in relation to that

2.3 Filming System

Flapping was recorded using 2 synchronized high-speed cameras (Fastcam SA-3_120K, Photron inc.) fitted with an 85mm lens and set to film at 500 fps (Exp 1/5000, resolution 1024x1024 pixels). The cameras were positioned above the flapper on opposite ends. Two infrared LED floodlights (ELIMEC Ltd) covered by a diffusive screen were placed underneath the flapper to provide better visual contrast in the recorded films ([Fig. 1b](#)). The cameras were spatially calibrated using an 8 cm-long wand and the “easywand5” software file from the MATLAB archives.

2.4 Data Analysis

Digitization

Digitalization of the seven points in each film frame was performed with the DLTdv5 software from MATLAB. Three landmarks on the leading edge (wb, mj, and wt) were used to define a relatively rigid plane throughout 3D space and the deviation of the four remaining landmarks (RP, MP, CuA, and AA) from that plane were calculated (see below) to describe the deflection of the trailing edge due to wing compliance (figure 2a).

Deleted: constant
Deleted: while
Deleted: defined
Deleted: Digitized landmarks helped track the position and orientation of trailing edge relative to the leading edge to extract flapping kinematics and wing deformation magnitudes.
Deleted: .

Normalized Flapping Cycle and Lift Force

All measurements were based on three flapping cycles. To control for variance in cycle duration, we divided the serial numbers of each film frame by the number of frames within a flapping cycle to give a non-dimensional time scale of flapping cycles labeled 0-3. Lift force was

calculated by the load cell measuring the weight every 10 milliseconds. All weights measured over the duration of the 3 flapping cycles were averaged together and converted to Newtons.

Wing Deformation

Wing deformation was measured only on the right wing in every trial (each trial consisted of flapping a pair of wings). We defined a wing-fixed Cartesian coordinate system using three leading-edge landmarks (wb, mj, and wt). The three points represent an instantaneous plane in 3D space given that the leading edge is relatively rigid. The perpendicular distance of the four trailing edge points was then calculated in relation to that plane to find the chordwise deflection. The deflection from the rigid plane defined the local wing camber while the spanwise difference in magnitude (gradient) between each point's deflection define the wing-twist.

To define the wing's coordinate system, two vectors were found within the wing's rigid plane. One connecting points wb to wt and one connecting wb to mj. A vector normal to both (hereby Z_w axis) was then defined by the cross-product: $Z_w = \vec{wt} \times \vec{mj}$. Due to inaccuracies in depth perception, the DLTdv5 defined the wt vector as negative in relation to the mj vector. The resulting cross-product was thus a negative Z_w meaning that the positive normal force direction is defined as the direction of the ventral side of the wing while the negative normal force is defined as going towards to dorsal side. The chordwise axis (Y_w) was then defined by the cross-product: $Y_w = \vec{wt} \times Z_w$. All vectors were then converted to unit vectors. These vectors were then used as a rotation matrix to transform all data point on the wing from the coordinate system of the cameras to the wing's frame of reference. The transformation of a given point P from the frame of reference of the camera to the frame of reference of the leading edge (P') is:

$$P' = \begin{bmatrix} wt_x & wt_y & wt_z \\ Y_{wx} & Y_{wy} & Y_{wz} \\ Z_{wx} & Z_{wy} & Z_{wz} \end{bmatrix} \begin{bmatrix} P_x \\ P_y \\ P_z \end{bmatrix}$$

The procedure was repeated for each film frame using a custom written Matlab code. By definition, the Z_w component of the transformed data points is the deflection out of the plane of the rigid leading edge.

Deleted: , relative to the leading edge

Deleted: to

Deleted: the

Deleted: leading edge

Deleted: leading

Deleted: edge

Deleted: made

Deleted: The

Deleted: force axis

Deleted: Z

Deleted: , lateral

Deleted: Y

Deleted: defined by the leading edge

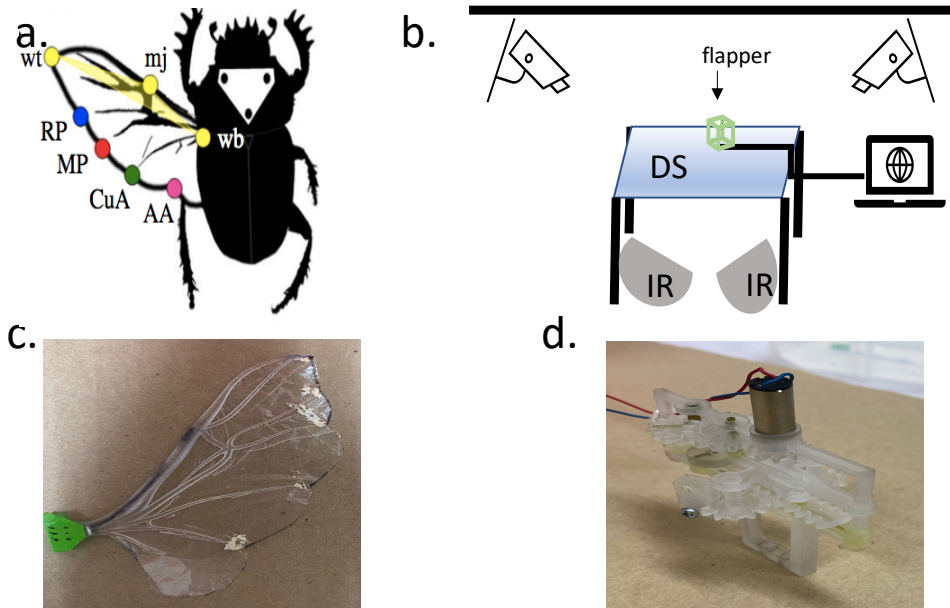


Figure 1. Methodology. (a) An illustration obtained from Meresman *et al.* (2020) denoting the landmarks used to extract flapping kinematics and wing deformation of the trailing edge. The rigid plane of the leading edge is defined as the instantaneous 3D plane comprised of wb (wing-base; in our case, the gear of the flapper), mj (marginal-joint), and wt (wing tip). Landmarks on the trailing edge were denoted as AA (Analis-Anterior vein), Cu (Cubitus-anterior vein), MP (Media-posterior vein) and RP (Radius-posterior vein). (b) Schematic representation of the experimental set-up. (c) Synthetic wing replica 5:1 scale-up of Protaetia Cuprea wing. (d) The flapper instrument, without the wings attached.

Deleted: Y.
 Deleted: and G. Ribak's paper presenting
 Deleted:
 Deleted: Protaetia Cuprea's digitized
 Deleted: L
 Deleted: Trailing
 Deleted: was
 Deleted: defined
 Deleted: 1:6

3. Results:

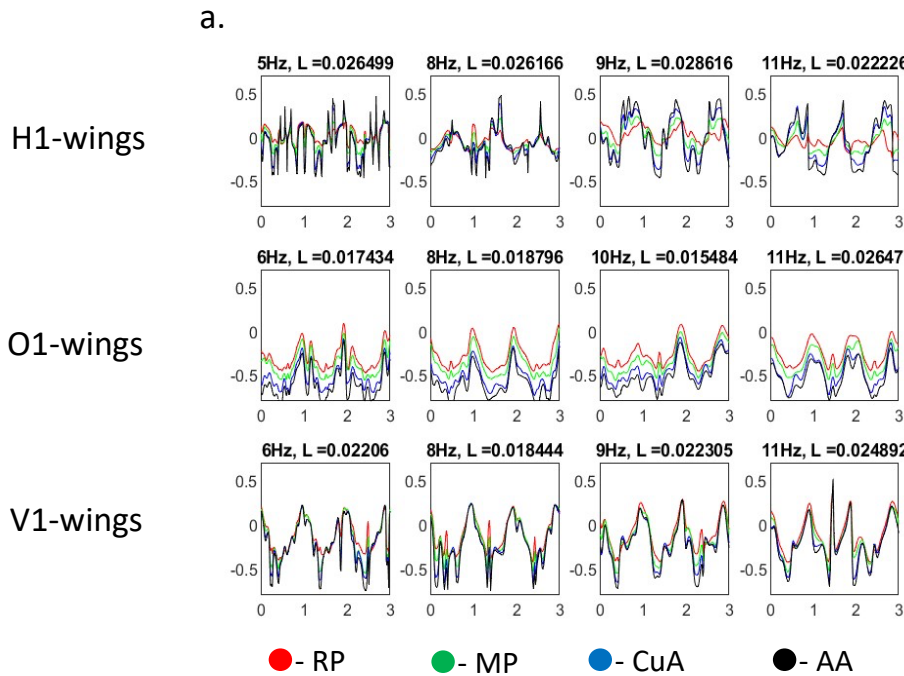
3.1 Wing Deformation –

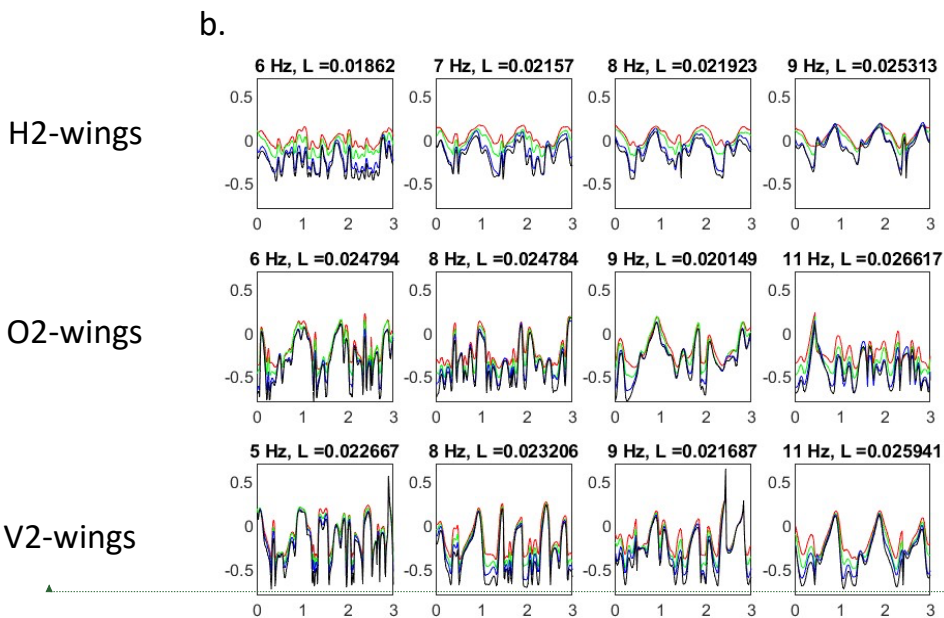
Throughout the flapping cycle of all trials, the four TE landmarks (RP, MP, CuA, and AA seen in figures 1a) exhibited a clear cyclic deformation pattern consistent with the flapping kinematics. Apart from the H1-wing flapping at 8Hz (Figure 2a, first row second column) whose deflection followed the direction of the wing flap resulting in positive camber, the remainder of the trials upon downstroke (defined here as flapping in a forward direction relative to the flapper) showed TE landmarks to be deflected towards the dorsal side of the wing while upon upstroke (defined here as flapping in a backward direction towards the flapper) the landmarks deflected towards the ventral side of the wing. Chordwise deformation was thus found to always be opposite to the wing's direction of movement resulting in negative camber irrespective of the wing types, except for the H1-wing at 8Hz. Additionally, only in H1 wings of 9Hz and 11Hz (figure 2a, row 1 columns 3 and 4) was there a symmetrical reflection about the y-axis to denote equal elasticity of both the ventral and dorsal sides of the specific wing as opposed to the remainder of the trials whose deflection never fully surpassed the LE to the ventral side.

Magnitude of the wing deflection for each point at mid-stroke relative to the LE, seen by the deviation from the y-axis 0 mark, demonstrated a clear spanwise gradient (wing twist) within the chordwise deformation. The landmark AA (represented by the black line) had the greatest deviation while RP (represented by the red line) had the least. This indicates ascending spanwise and chordwise rigidity from the proximal point AA being the least rigid to the more distal point, RP, being the most rigid. When comparing between wing sets, horizontally veined (H) wings from both trials displayed the greatest resistance to chordwise deformation while those with vertical (V-wings) and rounded (O-wings) geometry veins showed no significant differences regarding their compliance. H and O wings did, however, seem to translate to having greater spanwise gradients seen by the more robust separations between relative deformation coefficients of each landmark. This suggests a steeper increase in spanwise rigidity relative to each point in H and O wings when ascending from the proximal to distal edge.

3.2 Wingbeat Frequency and Lift–

Raising the wingbeat frequency (presented at the top of each graph in Hz) resulted in inconclusive fluctuations of generated lift-force hereby suggesting that wingbeat frequency had no significant effect on any of the wings' lift generation capabilities. Even upon positive camber as noted in the H1 wing at 8Hz, there was no apparent increase to lift generation. In addition, wingbeat frequency had no apparent effect on chordwise or spanwise wing deflection when comparing between the same sets (i.e. H1 wing deformation at all frequencies in figure 1 fluctuates about the 0.5 mark).





Moved down [1]: 4. Discussion and

Figure 2a. and 2b. Trials 1 and 2 refer to flapping of different batches of the same wing sets (i.e. trial 1 uses one batch of H wings and trial 2 uses another batch of H wings). Each individual graph displays normalized deformation of the trailing edge relative to the leading edge as a function of wing set. Each row depicts a different wing set (Horizontal (H), Round (O), or Vertical (V)) and each column depicts ascending wingbeat frequency (seen on top of each individual graph in Hz). Deformation of each landmark is color coded as; RP in red, MP in green, CuA in blue, and AA in black. Lift force (L) on the top of each individual graph represents the lift force measured in Newtons.

4. Discussion and Conclusion:

As mentioned in previous studies, oversimplified mathematical models incorrectly assume that larger individuals of the same species have an isometric magnification of wings^{3,5}. This inability to predict results by simple scaling of the model makes it difficult to calculate the change in forces that emerge from variations of wing rigidity. In an attempt to gain insight as to the relationship between wing form and function in its interplay in the evolution of flexible insect wings, we recreated 3 isometric models of *P. cupreia* wings, where, by solely modifying

Moved (insertion) [1]

Deleted: by Gal Ribak,

Deleted: benefits of

Deleted: elasticity versus wing rigidity

Formatted: Font: Italic, Complex Script Font: Italic

the shape of the veinal cross-sectional area, we provided a method for controlled manipulation of wing compliance.

Our study corroborated the hypothesis that subtle changes in wing vein cross-section geometry results in noteworthy differences in wing compliance during flapping. Nevertheless, we found no sufficient evidence to infer a positive correlation between wingbeat kinematics coupled with varying degrees of rigidity, on lift-force generation. When raising the wingbeat frequency within the same set of wings, we would expect a steady squared proportionate increase in lift force generated, granted all other variables remain constant, seen by the lift force equation: $L = C_L \times \frac{\rho \times V^2}{2} \times A$ (where L = lift force, C_L = lift coefficient, ρ = air density, V^2 = velocity, and A = area of the wing). This was not observed, however, when comparing the frequency differences within a set. Most likely this is due to the loss of aerofoil shape as the TE buckled under the air's force translating to a negative camber. The lift coefficient mentioned above depends on the angle of attack and camber. The wings in our study were mounted on the flapper at an angle of attack 90°, in the hope that the wing deformations will reduce the effective angle of attack to lower ones with higher lift coefficients. Unlike the documented positive wing camber in free-flying beetles which was achieved via TE deflection in the direction of the flapping to promote lift, our graphs depict an opposite trend in the synthetic wings^{3,4}.

Wing buckling at the trailing edge thus, reversed the expected camber, kept the angle of attack high and significantly reduced the overall wing area exposed to the air. The result of the combined factors greatly impacted (decreased) aerodynamic properties and also rendered our lift force measurements inconclusive and inaccurate. On the other hand, however, the H1 wing flapping at 8Hz was an outlier suggesting that negative camber may not be the sole culprit for the lack of lift-generation. Even though it showed positive camber, the lift-force measured did not show any particular improvement.

Furthermore, aside from H1 wings at 9Hz and 11Hz, uniform reflection of the deformation coefficients about the y-axis was not observed. This entails dorso-ventral asymmetry potentially preventing the formation of functional aerofoil structures to promote lift both during upstroke and downstroke which is not entirely compliant with data depicting flexural stiffness of free-flying rose chafer wings^{1,4}. It is important to note that specifically for

Deleted: to directly alter

Deleted: In o

Deleted: , our

Deleted: held true i

Deleted: n that we observed

Deleted: rigidity

Deleted: when comparing between normalized TE deviations in relation to the LE of each wing set

Deleted: , m

Deleted: ,

Deleted: impacting

Deleted: qualities

the H-wing sets, two different batches, one of which was older, were used. This possibly caused degradation of the synthetic material in the older batch, effecting its resilience and thus also tampered with the frequency, lift and deformation we recorded between the H-wing sets.

Overall, our findings did show that veins and flexural rigidity play a significant role in wing deformation. Moreover, in order to better mimic the kinematics of free-flying rose chafer wings we see that solely manipulating the rigidity through vein geometry is insufficient.

Wootton (2020) mentions the accountability that the wing cuticle as well as vein corrugation holds on wing twist and wing camber. He also stresses the necessity of experimentation using physical replicas and refining them to better resemble results recorded in free-flight experiments to overcome the limitations mathematical predictions have^{2,6}. This study thus highlights the importance of the interaction between the complex mechanical properties found in actual wings. Ultimately, in order to find more viable and reproducible measurements pertaining to the lift force generated in response to wing rigidity, it would be beneficial to improve the capacity of the synthetic wings to resist negative camber. Likewise, improvements to the flapper should be made to make it more durable as it frequently broke down, hindering the maximum wingbeat frequency we can provide and the flapping symmetry between sets.

Deleted: YEAR

References:

- (1) Meresman, Y.; Ribak, G. Elastic Wing Deformations Mitigate Flapping Asymmetry during Manoeuvres in Rose Chafers (*Protaetia Cuprea*). *Journal of Experimental Biology* **2020**, jeb.225599. <https://doi.org/10.1242/jeb.225599>.
- (2) Wootton, R. J. Support and Deformability in Insect Wings. *Journal of Zoology* **1981**, 193 (4), 447–468. <https://doi.org/10.1111/j.1469-7998.1981.tb01497.x>.
- (3) Meresman, Y.; Ribak, G. Allometry of Wing Twist and Camber in a Flower Chafer during Free Flight: How Do Wing Deformations Scale with Body Size? *R. Soc. open sci.* **2017**, 4 (10), 171152. <https://doi.org/10.1098/rsos.171152>.
- (4) Meresman, Y.; Husak, J. F.; Ben-Shlomo, R.; Ribak, G. Morphological Diversification Has Led to Inter-Specific Variation in Elastic Wing Deformation during Flight in Scarab Beetles. *R. Soc. open sci.* **2020**, 7 (4), 200277. <https://doi.org/10.1098/rsos.200277>.
- (5) Combes, S. A.; Daniel, T. L. Flexural Stiffness in Insect Wings I. Scaling and the Influence of Wing Venation. *Journal of Experimental Biology* **2003**, 206 (17), 2979–2987. <https://doi.org/10.1242/jeb.00523>.
- (6) Wootton, R. The Geometry and Mechanics of Insect Wing Deformations in Flight: A Modelling Approach. *Insects* **2020**, 11 (7), 446. <https://doi.org/10.3390/insects11070446>.